

SH 138: a compact H II region excited by a very young cluster region excited by a very young cluster

L. Deharveng, Annie Zavagno, D. Nadeau, J. Caplan, M. Petit

▶ **To cite this version:**

L. Deharveng, Annie Zavagno, D. Nadeau, J. Caplan, M. Petit. SH 138: a compact H II region excited by a very young cluster region excited by a very young cluster. Astronomy and Astrophysics - A&A, 1999, 344, pp.943-954. hal-03562786

HAL Id: hal-03562786

https://amu.hal.science/hal-03562786

Submitted on 18 Feb 2022

HAL is a multi-disciplinary open access archive for the deposit and dissemination of scientific research documents, whether they are published or not. The documents may come from teaching and research institutions in France or abroad, or from public or private research centers.

L'archive ouverte pluridisciplinaire **HAL**, est destinée au dépôt et à la diffusion de documents scientifiques de niveau recherche, publiés ou non, émanant des établissements d'enseignement et de recherche français ou étrangers, des laboratoires publics ou privés.



Distributed under a Creative Commons Attribution 4.0 International License

Astron. Astrophys. 344, 943–954 (1999)

ASTRONOMY AND ASTROPHYSICS

Sh 138: a compact H II region excited by a very young cluster⋆,⋆⋆

L. Deharveng[1], **A. Zavagno**[1], **D. Nadeau**[2], **J. Caplan**[1], **and M. Petit**[1]

[1] Observatoire de Marseille, 2 Place Le Verrier, F-13248 Marseille Cedex 4, France (deharveng@obmara.cnrs-mrs.fr)
[2] Observatoire du Mont Mégantic et Département de Physique, Université de Montréal, C.P. 6128, Succ. Centre-ville, Montréal, QC, Canada H3C 3J7 (nadeaud@ere.umontreal.ca)

Received 28 July 1998 / Accepted 14 January 1999

Abstract. We present a photometric and spectroscopic study of the compact H II region Sh 138 and its associated stellar cluster. The positions and *BVRIJHK* magnitudes are obtained for more than 400 stars over a field of about 4′ square centred on the H II region. Sh 138 is excited by a cluster of young massive stars. At the cluster's very centre are at least four O–B2 stars separated by less than 4″. The brightest of these, both in the visible and the near infrared, exhibits a spectrum similar to those of the more massive Herbig Ae/Be stars. This star, our No. 183, is overluminous by a factor of 2.5 in the visible and four in the near IR with respect to the O9.5 V star required to account for the ionization level of the H II region. However star 183's position in the $J-H$ versus $H-K$ diagram does not indicate a near-IR excess. We suggest that this star is a young massive object belonging to a binary or multiple system.

The stellar cluster associated with Sh 138 is very reminiscent of the Orion Trapezium cluster: it is centrally peaked around several massive stars, and is dense – more than 550 stars pc^{-2} at its centre. The visual extinction in the cluster varies between 5 mag and more than 35 mag; large variations are observed over very small scales (for example, more than 20 mag over less than 4″ among the central massive stars).

Key words: stars: pre-main sequence – ISM: H II regions – ISM: individual objects: Sh 138 – Galaxy: open clusters and associations: individual: Sh 138 – infrared: stars

1. Introduction

The O–B2 stars that ionize H II regions are more massive than about 8 $M_{\odot}$. Little is known about the formation of such massive objects because few are observed being formed. According to the classical Salpeter (1955) IMF, only one O star is formed for about 250 G stars. These few massive stars last only a very short time in their formative phase. So it is not surprising that no massive protostellar object lies in the solar vicinity to give us a close-up view. Furthermore, stellar models by Palla & Stahler (1990), Beech & Mitalas (1994) and Bernasconi & Maeder (1996) show that an object more massive than 7–10 $M_{\odot}$ does not go through an optically-visible pre-main-sequence phase, as do Herbig Ae/Be stars or T Tauri stars, but is still accreting material when it starts burning its central hydrogen, and remains hidden behind an accreting envelope during a large fraction of its main-sequence lifetime. Hence the morphology of these objects is unknown. Does the accretion proceed via a disk, and is it accompanied by ejection phenomena? These signatures of extreme youth for intermediate and low mass stars, if present for massive stars already on the main sequence and ionizing the surrounding material, would probably influence the very first phases of the evolution of H II regions, i.e. the ultracompact and compact phases.

In order to better understand the evolution of massive stars towards the main sequence, we have begun a study of the stellar content of ultracompact and compact H II regions. We present here the case of Sh 138 (Sharpless 1959), which we originally believed to be a classical compact H II region excited by one optically-visible main-sequence star but which we find to be associated with a very populous cluster containing at least one hot star which exhibits pre-main-sequence characteristics.

The region and its environment are described in Sect. 2. In Sect. 3, *BVRIJHK* photometric observations are presented and the nature of various stellar objects is discussed. Sect. 4 deals with spectroscopic observations. Observed characteristics of this region are discussed in Sect. 5, and conclusions are drawn in Sect. 6.

2. Description of the region

Sh 138 is a compact H II region located at a distance of 5 ± 1 kpc (see Sect. 5.1 for a discussion of the distance). Fig. 1 shows the Hα and radio continuum emission of the ionized gas. The radio map was obtained by Felli & Harten (1981) at 4.99 GHz, with a resolution of 6″; another map was obtained by Fich (1993)

Send offprint requests to: L. Deharveng

⋆ Based on observations done at the Observatoire de Haute Provence and the Observatoire du Pic du Midi, France, and at the Canada-France-Hawaii Telescope. The CFHT is operated by the Centre National de la Recherche Scientifique of France, the National Research Council of Canada and the University of Hawaii.

⋆⋆ Table 1 is available in electronic form at the CDS (via anonymous ftp to cdsarc.u-strasbg.fr or via http://cdsweb.u-strasbg.fr/Abstract.html) as well as at http://www-obs.cnrs-mrs.fr/matiere/sh138-t1.html

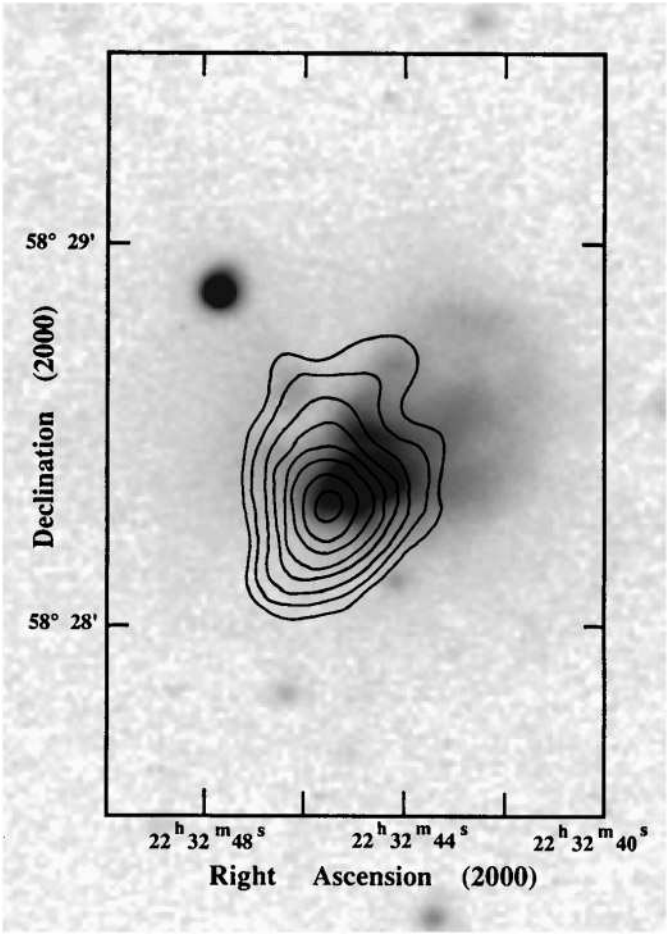


Fig. 1. Radio emission (Felli & Harten 1981) of the H II region Sh 138, superimposed on an Hα frame obtained with the 120-cm telescope at the Observatoire de Haute Provence

at 4.89 GHz, with a resolution of $13''$; these maps are in agreement, in particular for the position of the radio emission peak at α_{2000} = $22^{\rm h}\ 32^{\rm m}\ 45\overset{\rm s}{.}6$ and δ_{2000} = +58° 28′16.″8.

An IR source (IRAS 22308+5812) is detected in the direction of the radio source. Its luminosity $L_{\rm IR}$, in the range 6–8 10^4 $L_\odot$ according to Simpson & Rubin (1990) and Chan & Fich (1995) for a distance of 5 kpc, suggests the presence of hot massive stars. ISO-SWS measurements (Roelfsema et al. 1996 and P. Cox, private communication) confirm the IRAS flux values obtained for this region. Its 3–20 μm spectrum exhibits the unidentified IR emission bands (Jourdain de Muizon et al. 1990; Zavagno et al. 1992; Roelfsema et al. 1996) commonly attributed to carbonaceous compounds (Léger & Puget 1984; Allamandola et al. 1985). This spectrum also shows the atomic fine-structure lines of [Ar II], [Ar III] and [Ne II] emitted by the ionized gas.

The molecular cloud associated with this region has been mapped by Johansson et al. (1994) near 100 GHz with a HPBW of $38''$. The core of the molecular cloud (i.e. the position of the CS emission peak) lies $24''$ south-east of the H II radio centre. Molecular emission extends to the north, in the direction of the H II region. The red wing of the CO emission may be slightly extended (L. Johansson, private communication) but higher resolution data are needed to confirm the presence of a molecular outflow.

Wouterloot et al. (1993) report the possible detection of a weak H_2O maser in the direction of the IRAS source; here again, new observations are needed to confirm this.

3. Photometry

3.1. Optical observations

We obtained B, V, R and I frames with the 2-m telescope of the Observatoire du Pic du Midi. The 1024×1024 19-μm-square pixels of the Thomson CCD were binned two-by-two. The resulting scale is $0\overset{''}{.}485$ per binned pixel. Two sets of frames were obtained, on the nights of 1993 November 21 and 25; the exposure times were 600 s, 400 s, 200 s and 200 s, respectively in B, V, R and I. The FWHMs of the PSFs are all $1\overset{''}{.}1$. Photometric calibration (colour equations, absolute flux calibration and atmospheric extinction coefficients) was done by observing the clusters NGC 7790 (Christian et al. 1985) and M 67 (Chevalier & Ilovaisky 1991). We have reduced all the frames using the DAOPHOT stellar photometry package (Stetson 1987). Our final R and I magnitudes are in the Cousins system (often referred to as $R_{\rm C}$ and $I_{\rm C}$).

We obtained an Hα frame (Fig. 1) at the 120-cm telescope of the Observatoire de Haute Provence on the night of 1990 September 23 with an RCA CCD having 512×323 pixels; the scale is $0\overset{''}{.}85$ per pixel. The exposure time was 600 s, and the FWHM of the PSF was $3\overset{''}{.}0$.

3.2. Near IR observations

We observed Sh 138 in the near IR at the 3.6-m Canada-France-Hawaii telescope on the night of 1996 July 1 (UT), using the Montreal IR camera MONICA (Nadeau et al. 1994). The detector is a NICMOS 3 with 256×256 pixels; the scale is $0\overset{''}{.}246$ per pixel. Frames were obtained through the J (1.25 μm, FWHM 0.29 μm), H (1.65 μm, FWHM 0.31 μm) and K (2.20 μm, FWHM 0.40 μm) broad-band filters with total integration times of 640 s, 320 s, and 60 s respectively.

Calibration was done with observations of six UKIRT standards[1]. These observations were used to determine both the atmospheric extinction coefficients and the colour equations of our photometric system. To adequately determine the photometric transformation coefficients, it is necessary to observe standards covering the full range of colour we are interested in. The 'provisional faint standards' FS 23, FS 24, FS 28 and FS 30 are rather blue. The bright standards S-R 3 and Oph S1 are sufficiently red, but are too bright to be observed in the usual manner without saturation of the detector, so they were observed out of focus. In the present paper all the J, H and K magnitudes are given after transformation to the UKIRT system.

[1] http://www.jach.hawaii.edu/UKIRT.new/astronomy/standards.html

3.3. Images of the field

Fig. 2a is a composite colour image created from the B, V and R images, with the B component in blue, the V in green and the R in red. The Sh 138 nebulosity is clearly seen thanks to its Hα emission in the R filter. Fig. 2b is a composite colour image created from the J, H and K frames, these being represented by blue, green and red respectively. The differences in colour of the stars in Fig. 2b are mainly due to differences in reddening and only slightly to differences in intrinsic colour (we shall show in Sect. 3.4 that very large extinction variations are observed from star to star).

The stars discussed in the text are identified in Fig. 3 by the same numbers as in Tables 1 and 2.

3.4. Results

Magnitudes were determined by PSF fitting using DAOPHOT. All the frames, especially those in the near IR, exhibit a highly non-uniform nebular background which hampers accurate photometry. The iterative procedure described in Deharveng et al. (1992) was used to reduce these variable-background frames. The frame coordinates of the stars were converted to right ascension and declination as explained in the Appendix.

Table 1[2] gives the J2000 positions, V, $B-V$, $V-R$, $R-I$ and $V-I$ obtained for 424 stars in the $4' \times 4'$ field centred on Sh 138. The positions are given both as 'standard' coordinates X, Y in arcminutes with respect to a field centre at $22^{\rm h}32^{\rm m}45\overset{\rm s}{.}6$, $+58^\circ 28' 16\overset{''}{.}8$, and as equatorial coordinates. There are 126 stars which are detected in all four bands. The magnitude limits, for stars with fairly uniform backgrounds, are about 21, 21.5, 21 and 20 in B, V, R and I respectively. Table 1 also gives K, $J-K$, $J-H$ and $H-K$ which we have measured for 184 stars in the $1' \times 1'$ field centred on Sh 138. Of these 184 stars, 108 have been detected in all three bands; the faintest stars we detect are of approximate magnitudes 19.5 in J, 18 in H and 17 in K. However the sample is not complete up to these limits, the faint stars being more difficult to detect in front of bright, non-uniform nebulosity.

Table 2 gives the coordinates, the magnitudes and the colours of the stars discussed individually in the text.

A cluster is very conspicuous in the IR frames at the same position as the emission nebula which is seen in the R and Hα frames. Star 183, bright in both the visual and the near IR, is located at the very centre of this cluster. It is a good exciting source candidate for Sh 138. We shall show that it is not a classical main-sequence star.

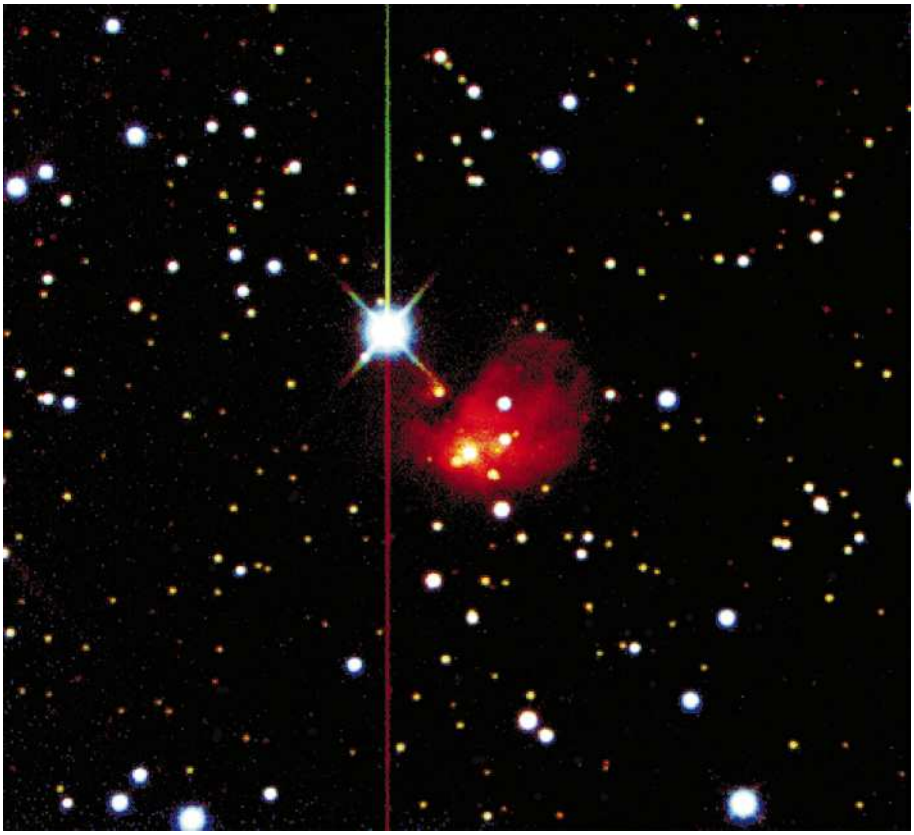
Firm conclusions about the stellar content of the exciting cluster are difficult to reach from the photometry alone because i) the distance of the cluster is uncertain and ii) young stars may have non-typical luminosities and colours. Fig. 4 shows the V versus $B-V$ and V versus $V-I$ diagrams obtained for the stars in the $4' \times 4'$ field. We have drawn the main sequence assuming a distance of 5 kpc and no extinction, and also with a colour excess E_{B-V} = 0.9 mag representing the foreground extinction due to interstellar dust not directly associated with the Sh 138 complex. The absolute magnitudes M_V are from Vacca et al. (1996) for O to B0 stars and from Schmidt-Kaler (1982) for later type main-sequence stars. We have also drawn the interstellar reddening lines (according to Mathis 1990, with $R_V = 3.1$), originating from an O9.5 V star (a likely spectral type for the main exciting star; see Sect. 5.2) and from a B2 V star; their lengths correspond to an E_{B-V} of 3 mag; the dashed lines on both sides of the B2 V reddening line correspond to the ± 1 kpc uncertainty in the distance. Star 183, at the centre of the cluster, appears to be the most massive and luminous star; its extinction A_V is ~ 7.6 mag. The nearby star 216 has an $A_V \sim 6.9$ mag. A number of reddened stars (43, 122, 136, 229, 246, 266 and 387, with A_V in the range 5–7 mag) are probably relatively massive stars associated with the cluster. Bright low-extinction stars, such as stars 8 and 375, are probably foreground stars, in which case they are less luminous than they seem to be. The V versus $V-I$ diagram confirms the extinctions derived from the V versus $B-V$ diagram, and extends the measurements to fainter and more reddened stars.

Fig. 5 presents the K versus $J-K$ and $J-H$ versus $H-K$ diagrams. We have also plotted the main sequence corresponding to a distance of 5 kpc, without extinction, and reddening lines according to the standard extinction law, with lengths corresponding to $E_{B-V} = 10$ mag. The main sequence, for the UKIRT photometric system, is from a list available on the Web (see previous address). These diagrams show more heavily reddened stars than are present in Fig. 4.

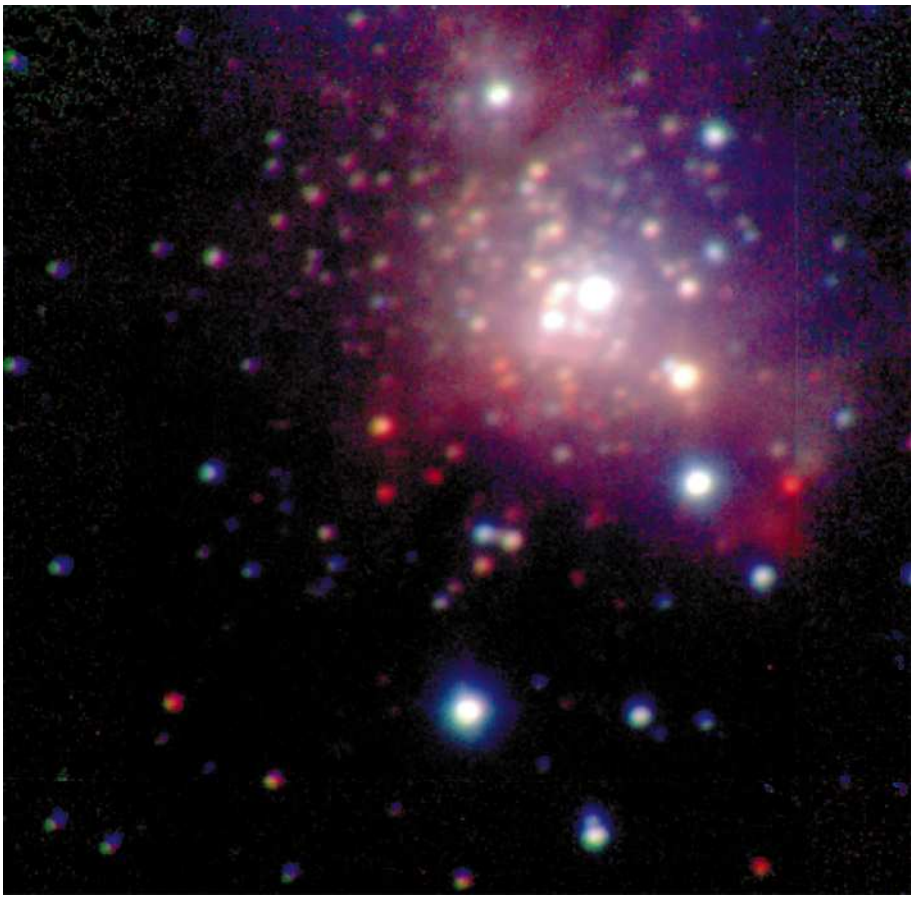
Stars 214 (in the very centre) and 291 are the most reddened stars detected in J, H and K, with $A_V \sim 28$ mag. The reddest star of the field in Fig. 2b, star 119, which is marginally detected in H but which is bright in K, is not present in these diagrams; given that K ~13.5 mag, that there is no detection in J, and assuming that it is a main-sequence star, we infer that it is less massive than an O9 V star, with an $A_V \geq 35$ mag. Most of the very red stars (119, 142, 153, 205, 244, 289, 291 and 323, with $A_V \geq 20$ mag) are located in the southern part of the cluster; they are very probably embedded in the molecular cloud or situated behind it. However a few very red stars are located in the centre of the cluster (star 214) or north of it (213, 225, 227). The bright central star, 183, clearly displays an excess luminosity for an O9.5 V star at 5 kpc. So does star 142; we shall return to this point in Sect. 5.2.

Fig. 5b shows that most of the stars are reddened main-sequence stars. But a number of them lie below the locus of these reddened main-sequence stars, indicating excess near-IR emission compared to a 'normal' reddened stellar photosphere. For faint stars this may be due to the scatter of the measurements (several stars lie above this locus as well); but this IR excess is real for relatively bright stars such as 142, 206, 214, 291 and 323. We estimate that about 15% of the stars detected in the three bands J, H and K present a near-IR excess. (The actual fraction of stars with an IR excess may well be higher, as a large number of highly reddened stars are observed only in K). Lada & Adams (1992) have shown that a reprocessing accretion disk can account well for a near IR excess of this amplitude. It is

[2] Table 1 is available in electronic form at the CDS



a



b

Fig. 2a and b. Composite colour images of Sh 138. North is up and east is left. **a** In the visible: B is blue, V is green and R is red; the frame size is $3\farcm89 \times 3\farcm52$. **b** In the near IR: J is blue, H is green and K is red; the frame size is $1\farcm18 \times 1\farcm18$. In the near IR we have used logarithmic units to enhance the low brightness objects

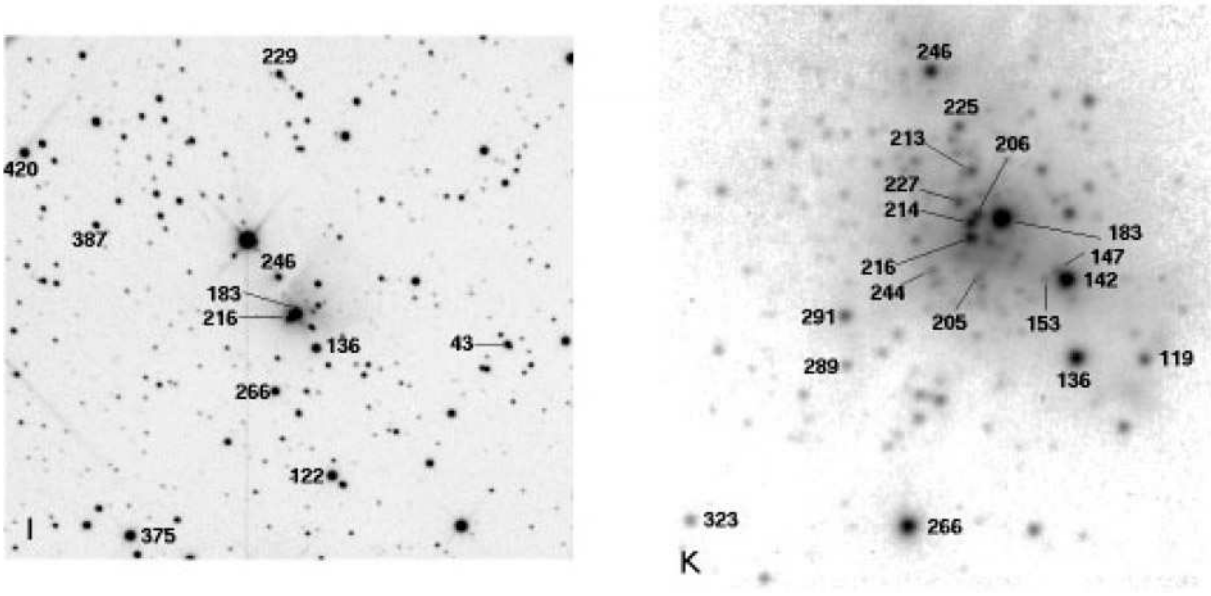


Fig. 3. I and K frames of Sh 138. The stars are identified by their numbers from Tables 1 and 2. The size of the I frame is $3\farcm94 \times 3\farcm67$, that of the K frame is $57'' \times 62''$

Table 2. Coordinates (J2000) and photometry of the stars mentioned in the text

No.	RA $-\ 22^{\rm h}$	Dec $-\ 58^\circ$	V	$B-V$	$V-R$	$V-I$	K	$J-K$	$J-H$	$H-K$
008	$32^{\rm m}30\fs43$	$30'06\farcs2$	13.65	+0.70	+0.40	+0.98				
043	$32^{\rm m}34\fs23$	$28'06\farcs4$	16.54	+1.60	+0.95	+1.95				
119	$32^{\rm m}43\fs49$	$28'06\farcs6$					13.52			+4.05
122	$32^{\rm m}43\fs73$	$27'13\farcs0$	14.98	+1.64	+0.95	+1.93				
136	$32^{\rm m}44\fs39$	$28'06\farcs9$	15.63	+1.60	+0.95	+1.94	11.32	+0.96	+0.71	+0.25
142	$32^{\rm m}44\fs52$	$28'15\farcs1$	20.66:			+3.55:	10.24	+3.55	+1.92	+1.63
183	$32^{\rm m}45\fs38$	$28'21\farcs6$	15.94	+2.11	+1.51	+3.01	9.24	+1.44	+0.83	+0.61
206	$32^{\rm m}45\fs69$	$28'22\farcs0$					12.36	+2.41	+1.14	+1.27
213	$32^{\rm m}45\fs77$	$28'26\farcs6$					13.40	+3.40	+2.05	+1.35
214	$32^{\rm m}45\fs78$	$28'21\farcs1$					12.03	+4.59	+2.57	+2.02
216	$32^{\rm m}45\fs79$	$28'19\farcs6$	18.08	+2.03	+1.39	+2.77	11.86	+1.36	+0.74	+0.62
225	$32^{\rm m}45\fs94$	$28'31\farcs2$					13.57	+3.40	+1.98	+1.42
227	$32^{\rm m}45\fs94$	$28'23\farcs2$					13.16	+3.18	+1.86	+1.32
229	$32^{\rm m}45\fs98$	$30'02\farcs7$	16.98	+1.66	+0.95	+1.94				
246	$32^{\rm m}46\fs31$	$28'37\farcs1$	18.33	+1.77	+1.18	+2.60	12.11	+1.35	+0.86	+0.49
266	$32^{\rm m}46\fs64$	$27'49\farcs2$	15.88	+1.68	+1.02	+2.02	11.36	+0.98	+0.79	+0.19
291	$32^{\rm m}47\fs46$	$28'11\farcs3$					13.57	+4.71	+2.66	+2.05
375	$32^{\rm m}54\fs51$	$26'49\farcs7$	13.52	+0.58	+0.28	+0.75				
387	$32^{\rm m}55\fs91$	$29'00\farcs9$	17.41	+1.91	+1.08	+2.27				
420	$32^{\rm m}59\fs61$	$29'32\farcs0$	14.90	+1.14	+0.63	+1.31				
$40''$-diameter										
diaphragm at	$32^{\rm m}45\fs60$	$28'21\farcs1$								
stars+nebulosity	.....						7.50	+2.04	+0.95	+1.09
stars alone	.....						8.29	+1.87	+1.00	+0.87
nebulosity alone	.....						8.21	+2.24	+0.90	+1.34

worth noting that for the central optically-visible stars 183 and 216 we do not detect such near-IR excesses.

Frogel & Persson (1972) did classical H and K aperture photometry of Sh 138 with diaphragms of diameter $15''$–$116''$. We have emulated the same aperture photometry using our J, H and K images. The results, with a $40''$-diameter diaphragm, are given in Table 2; they are in agreement (to better than 0.1 mag) with Frogel and Persson's measurements. But we are able to separate the contribution of the stars from that of the extended background emission thanks to our preliminary treat-

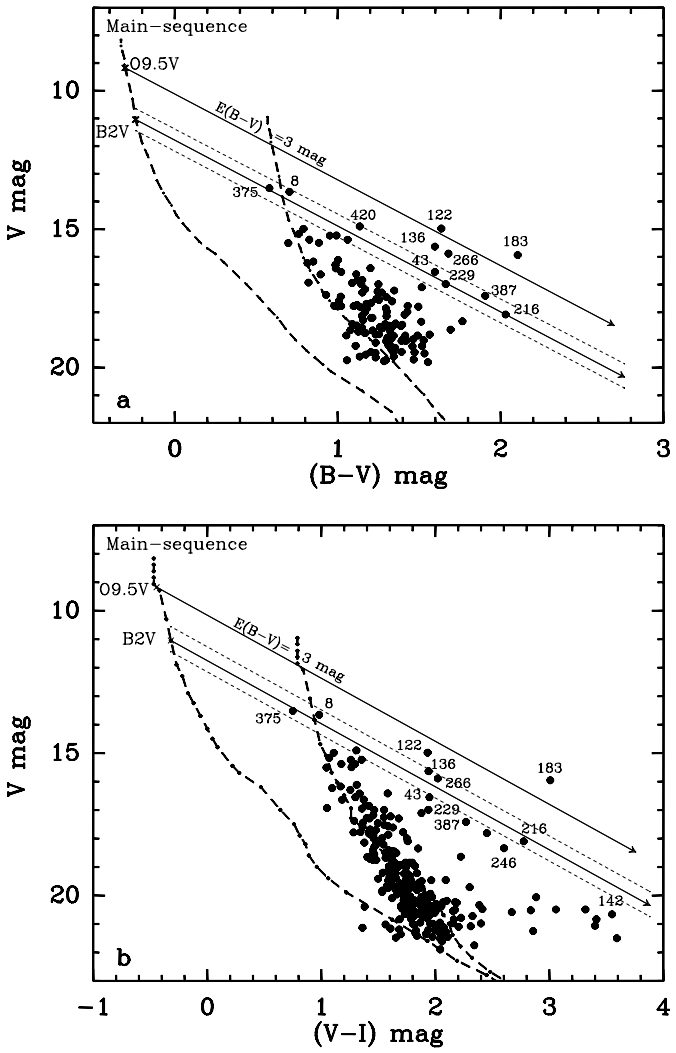


Fig. 4a and b. Colour-magnitude diagrams in the visible. **a** V versus $B-V$ and **b** V versus $V-I$. Long dashes: main sequence, for a distance of 5 kpc, with no extinction or a foreground extinction E_{B-V} = 0.9 mag; solid lines: reddening lines, corresponding to E_{B-V} = 3 mag, for O9.5 V and B2 V stars; short dashes: reddening lines for a B2 V star situated at 4 or 6 kpc

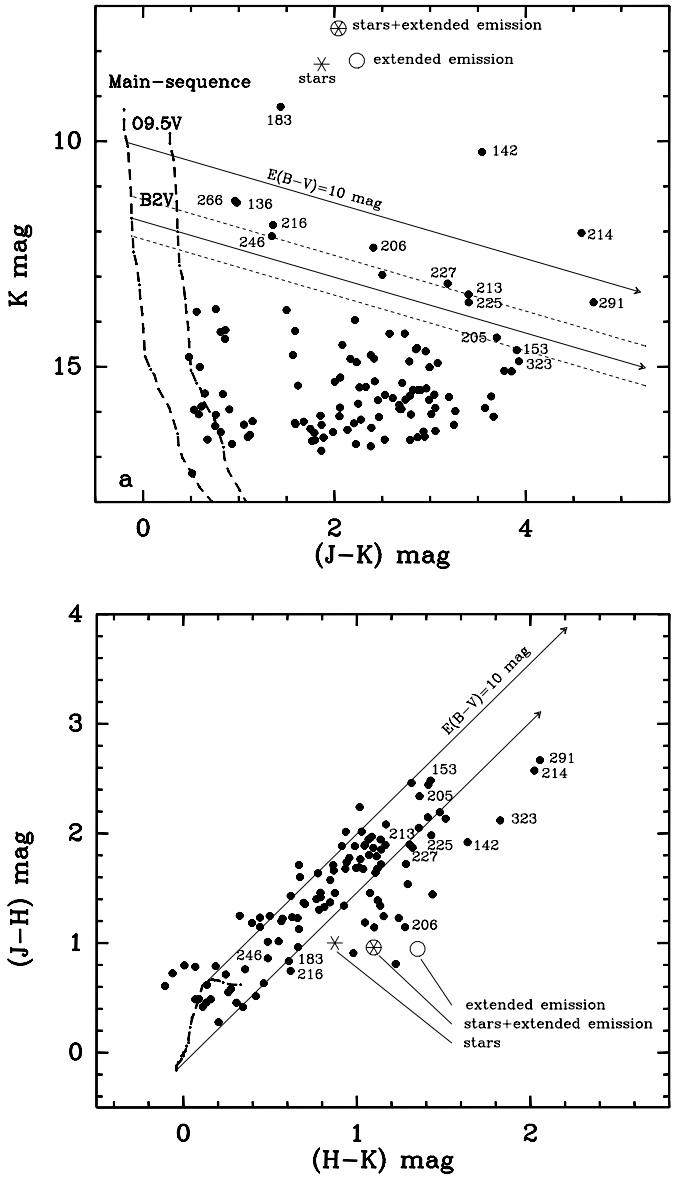


Fig. 5a and b. Colour-magnitude diagrams in the NIR. **a** K versus $J-K$; **b** $J-H$ versus $H-K$. The long dashes and the solid thin lines have the same meaning as in Fig. 4 but the lengths correspond to $E_{B-V} = 10$ mag. The large symbols represent aperture photometry obtained with a 40″ diaphragm centred on star 183; they refer to the stars contained in this diaphragm plus the non-stellar background emission, to the stars alone and to the background alone

ment using DAOPHOT to remove the non-uniform background (cf. Deharveng et al. 1992). Our results with this diaphragm, which includes a large fraction of the cluster's stars, are shown in Fig. 5. In K, the background emission is almost as strong as the integrated stellar emission and its colours are quite different. They are similar to those found by Sellgren (1984) for visual reflection nebulae, i.e. redder than the integrated stellar emission, showing that the reflected stellar light is not the only component of this background. Brγ emission of the ionized gas probably contributes in K, and small hot dust grains may also contribute at this wavelength. This shows the limitations of aperture photometry which, in this kind of region, very often includes a significant background contribution of uncertain origin.

4. Spectroscopy

4.1. Observations and reductions

We used the CARELEC spectrograph at the 193-cm telescope of the Haute Provence Observatory. Two 400-Å-wide spectral ranges were observed, one centred on Hα and one near 8600 Å. The slit dimensions are $3'' \times 5'$. Observations were made in October and November 1990, December 1993 and November 1994. The exposure time was one hour for each spectrogram, five of which were obtained in the Hα range and three in the

8600 Å range. The slit orientation was different for each spectrogram, allowing us to observe various parts of the H II region, but the slit always passed through the bright central star 183. The dispersion was 34 km s^{-1} per pixel in the Hα range, and 25 km s^{-1} per pixel around 8600 Å. The spectral resolution, given by the FWHM of neon and argon calibration lines, is about 80 km s^{-1} near Hα and 60 km s^{-1} near 8600 Å. The wavelength and photometric calibrations were performed as explained in Zavagno et al. (1994).

4.2. Results

Line emission from the Sh 138 H II region is seen along the slit in each spectral range, superimposed on a rather uniform extended emission. Near Hα, the [N II] lines at 6548 Å and 6584 Å, the He I line at 6678 Å and the [S II] doublet at 6717 Å and 6731 Å are also seen. The remarkable feature is the presence of extended Hα wings, observed only in the direction of star 183. We shall return to this point in Sect. 4.2.1. In the 8600 Å range, the spectrum is dominated by the hydrogen Paschen recombination lines (from P12 to P20), and by the O I line at 8446 Å. The Paschen lines are bright and very broad in the direction of star 183.

4.2.1. Spectrum in the direction of star 183

In order to determine the spectral characteristics of the star, we need to subtract the contribution of the H II region, which was assumed to be equal to the mean of the nebular signals on either side of star 183. The result is rather uncertain in the Hα range, as the nebular Hα is bright and non-uniform. The situation is less critical near 8600 Å where the contribution of the H II region is smaller. The resulting spectra of star 183 are shown in Figs. 6 and 7 in the Hα and 8600 Å ranges, respectively.

In the Hα range, the nebular emission lines, corrected for instrumental broadening, are narrow (FWHM = 40 km s^{-1}). A broad and intense residual Hα emission is present in the spectrum of star 183 (equivalent width 130 ± 20 Å and FWHM 105 km s^{-1}). The presence of extended wings on each side of Hα indicates velocities up to $\pm$ 500 km s^{-1} in the emitting zone (this result does not depend on the subtracted nebular contribution).

The helium emission line at 6678 Å is present in the stellar spectrum after subtraction of the nebular emission, and is broader than that emitted by the H II region. Such helium lines are also seen in the spectra of T Tauri and Herbig Ae/Be stars (Hamann & Persson 1992a,b).

Three absorption features at the position of known diffuse interstellar bands (DIBs; Jenniskens & Désert 1995) are seen at 6376 Å, 6614 Å and 8620 Å and seem to be associated with the star, as they are not seen in the spectrum of the H II region. This indicates that dust is located in the star's immediate vicinity. Such DIBs are also seen in the spectra of other massive young objects like MWC 1080, and MWC 137 which excites the compact H II region Sh 266 (Hamann & Persson 1992b; Deharveng unpublished data).

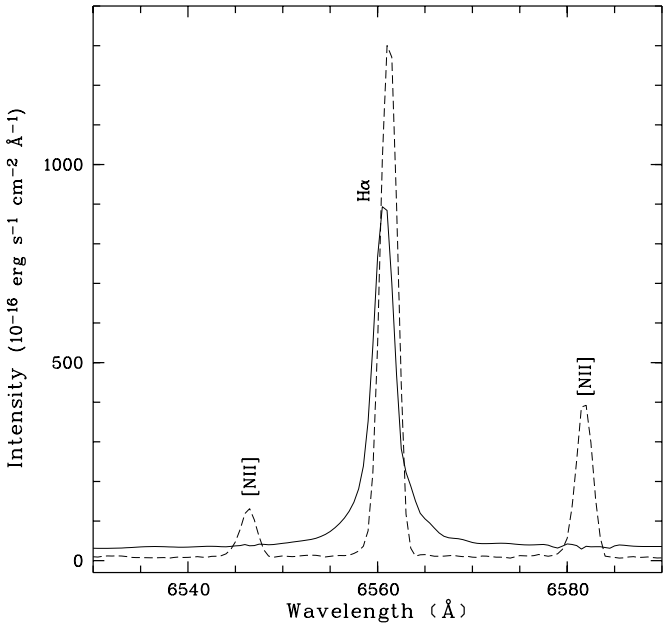


Fig. 6. Spectrum near Hα of star 183 (solid line) obtained *after subtraction of the nebular emission* (dashed line). Note the extended wings on each side of Hα

Fig. 7 shows that in the 8600 Å range the nebular emission lines are narrow and the contribution of the H II region is small. Table 3 presents the measured equivalent widths and fluxes for the main identified emission lines in the spectrum of star 183. The Paschen lines are bright (equivalent widths of about 2 Å) and broad (FWHM $\sim$ 240 km s^{-1}). The blending of the P13, P15 and P16 lines with the Ca II triplet lines is marginally visible in Fig. 7. In Fig. 8 we present the measured fluxes (not corrected for interstellar extinction) in the Paschen and Ca II lines observed in the direction of star 183. The fluxes of the blended Paschen lines have been estimated by interpolation between the unblended Paschen lines, then subtracted from the fluxes of the blends to give the Ca II and O I fluxes. These indirect measurements are followed by a colon in Table 3. The Ca II triplet fluxes show that these lines are optically thick (because if they were optically thin the 8498 Å, 8542 Å and 8662 Å line intensities would be in the ratios 1:9:5; cf. Herbig & Soderblom 1980).

If star 183 is a single object, its spectrum is comparable to those of the most massive YSOs described by Hamann & Persson (1992b). For example, the Ca II 8542 Å luminosity of $0.8 L_{\odot}$, the ratios F(O I 8446 Å)/F(Ca II 8542 Å) = 3.2 and F(P12)/F(Ca II 8542 Å) = 2.0 (for a distance of 5 kpc and corrected for an A_V of 7.6 mag), and the possible detection of N I lines near 8683 Å are typical of early-spectral-type objects (cf. Figs. 5 and 7 in Hamann & Persson 1992b).

In many respects, the spectrum of star 183 is very similar to that of IRS 4, the exciting source of the bipolar compact H II region Sh 106 (McGregor et al. 1984, who refer to IRS 4 as 'IRS 3'; these sources are clearly identified in Aspin et al. 1990). In IRS 4, as in star 183, the O I and Paschen lines clearly dominate the near IR spectrum, and Ca II emission is present but relatively faint.

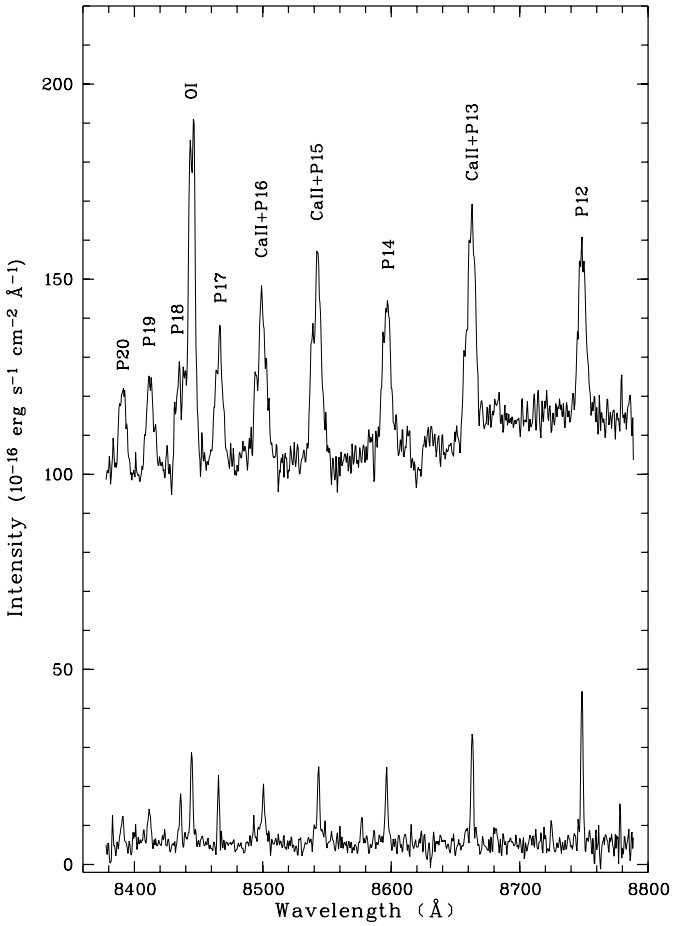


Fig. 7. Spectrum near 8600 Å of star 183 (*upper spectrum*) obtained *after subtraction of the nebular emission* (*lower spectrum*). Note the weakness of the nebular emission

4.2.2. The velocity of the H II region

We have measured the radial velocity of the ionized gas from the Hα, [N II] and [S II] emission lines. The mean velocity of the whole optical H II region is $V_{\rm LSR} = -50 \pm 2$ km s^{-1}. This agrees with the velocity of the associated molecular cloud, $V_{\rm LSR}({\rm CO}) = -52.0 \pm 1.0$ km s^{-1} (Blitz et al. 1982; Johansson et al. 1994).

The Hα velocity field of Sh 138, obtained by J. Boulesteix (private communication), shows the absence of supersonic velocities in the optical nebula.

Strong, uniform Hα emission is observed all along the slit at $V_{\rm LSR} \geq -30$ km s^{-1}. This velocity indicates that the emission comes from foreground ionized gas. Indeed, large field photographs (Dubout-Crillon 1976) show diffuse emission extending over several square degrees in this region.

4.2.3. Electron density in the H II region

We have used the task NEBULAR (Shaw & Dufour 1995), developed at the Space Telescope Science Institute, to derive the electron density in various parts of the optical H II region, using the intensity ratio of the [S II] lines at 6716 Å and 6731 Å. We obtain the highest electron density, $N_{\rm e}$ = 1000 cm^{-3}, in the immediate vicinity of star 183; $N_{\rm e}$ is in the range 500–600 cm^{-3} in the bright central parts of Sh 138, at less than 10″ (∼0.3 pc) from the exciting star; $N_{\rm e}$ drops to 200 cm^{-3} in the outer parts of the optical nebula. Felli & Harten (1981) found, from radio flux measurements, a density of 2500 cm^{-3} for the core of the H II region. This latter density depends on the assumed size for the compact H II region, size which is not well determined. In any case the two determinations indicate a relatively high-density medium near star 183.

Table 3. Emission line fluxes measured in the spectrum of star 183 (in the 8600 Å range)

Identification	$\lambda_\circ$ (Å)	EW (Å)	Flux (10^{-16}erg s^{-1}cm^{-2})
P20	8392.400	1.32	135±7
P19	8413.321	1.52	154±12
P18+O I	8437.958*	6.94	712±12
O I	8446.50	5.2:	540:
P17	8467.256	2.04	209±7
P16+Ca II	8502.487*	3.5	369±14
Ca II 8498 Å	8498.018	1.3:	138:
P15+Ca II	8545.384*	4.15	433±15
Ca II 8542 Å	8542.049	1.7:	180:
P14	8598.394	2.65	288±8
P13+Ca II	8665.021	3.7	414±20
Ca II 8662 Å	8662.140	1.0:	115:
P12	8750.475	2.72	316±14

* The wavelengths are those of the Paschen lines, but the equivalent widths and fluxes are those of the blends.

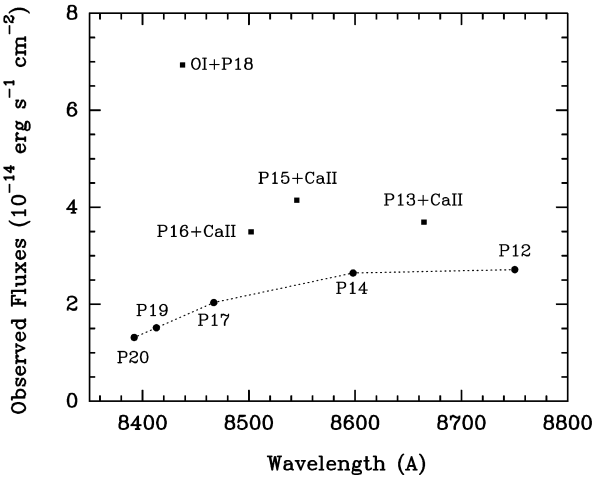


Fig. 8. Measured line fluxes in the direction of star 183. Blending of the P13, P15, P16 and P18 Paschen lines with the Ca II triplet and with O I is clearly seen

5. Discussion

5.1. The distance of Sh 138

The only distance estimate available for Sh 138 is its kinematic distance, which is 5.9 kpc. This is derived from the radial ve-

locity of its associated molecular material, $V_{\rm LSR}({\rm CO}) = -52$ km s^{-1} (Blitz et al. 1982), by using the Galactic rotation curve of Brand & Blitz (1993) with the standard values for the Galactocentric distance of the Sun, R_0 = 8.5 kpc, and the LSR's circular velocity $\theta_0 = 220$ km s^{-1}. Using a flat rotation curve beyond the solar circle ($\theta = \theta_0 = 220$ km s^{-1}) would result in a kinematic distance of 5.45 kpc.

The molecular clouds associated with the nearby compact H II regions Sh 138, Sh 148-149, Sh 152-153 and Sh 156 display similar velocities (Blitz et al. 1982); thus we assume that these regions lie close to each other. Except for Sh 138, the spectral types of their exciting stars are known, so photometric distances have been estimated using the absolute calibration of Vacca et al. (1996). These are 5.3 kpc for Sh 148, 5.9 kpc for Sh 149, 3.45 kpc for Sh 152, 4.5 kpc for Sh 153 and 5.1 kpc for Sh 156 (Caplan et al. 1999). This gives a mean photometric distance of 4.8 kpc for the group. If we had used the absolute calibration of Schmidt-Kaler (1982), the mean photometric distance would be 5.1 kpc.

Henceforth we adopt a distance of 5.0±1.0 kpc for Sh 138.

5.2. The ionization of the H II region

Sh 138 is a thermal continuum source (Kazès et al. 1975, Felli & Harten 1981, Gregory & Taylor 1986, Fich 1993). Its radio flux density allows us to estimate the number of ionizing photons per second, and hence the spectral type of its exciting star – assuming that a single main-sequence star dominates the ionization. This flux has been measured between 6 and 21 cm, both at low and high angular resolution; all the measurements agree and give $S_{\rm 5GHz} \sim 0.57$ Jy. Using Eq. 1 of Simpson & Rubin (1990) and a distance of 5.0±1.0 kpc, we derive an ionizing flux $N_{\rm Lyc} = (1.3 \pm 0.5)\ 10^{48}$ photons s^{-1}. According to Schaerer & de Koter (1997) this corresponds to an O9.5 V or B0 V star; and according to Vacca et al. (1996), who use the stellar models of Kurucz (1991), this indicates a B0 V. Note that the presence of more than one ionizing star would imply later spectral types.

On the other hand, the helium ionic abundance He^+/H^+ = 0.057, and the detection of faint [O III] 5007 Å emission (Deharveng et al. 1999), suggest that Sh 138 is similar to the compact H II regions Sh 93 and Sh 152, which are excited by an O9.5 V star and an O9 V star respectively. Thus we think that the spectral type of the main exciting star of Sh 138, if on the main-sequence, cannot be earlier than O9 V and can hardly be later than B0 V. Our best guess is O9.5 V.

The very centre of Sh 138 (radio and optical H II region and stellar cluster) contains at least four massive stars separated by less than 4″. Stars 183 and 216 are optically visible; star 183 is the brightest, both in the optical and the near IR. Stars 206 and 214 appear only in the near IR. One or more of these stars are obviously responsible for the ionization of the gas. The colour-magnitude diagrams (see Figs. 4 and 5) show that: i) star 183 is the brightest of the four stars; if an O9.5 V star, it is overluminous by about 1 mag in the visible and 1.5 mag in the near IR; ii) stars 206 and 216 may be classical B1 V stars; iii) star 214 also appears to be a very massive and overluminous object.

As to the nature of star 183, and the main exciting source of Sh 138, we hesitate between two possibilities:

• Star 183 is an O9–B0 main-sequence star, and is the main exciting source of Sh 138. But then this star is overluminous. This overluminosity can hardly be entirely due to errors in the distance (see Fig. 5a); it cannot be due to the presence of a disk because such a disk would certainly be detectable by a near-IR excess, which is not the case. The overluminosity is difficult to understand in the light of present-day evolutionary models in which young massive objects either evolve towards the main sequence at constant luminosity, or evolve up the main sequence (Bernasconi & Maeder 1996, their Figs. 2 and 5). One obvious possibility is that star 183 is a non-resolved binary (or multiple) system, its companion being a massive object too.
• Star 183 has already evolved and is a giant; a B0.5 III star would account for the ionization of hydrogen and would have the required luminosity. But it would be too cold to account for the ionization of helium (see Table 3 in Schaerer & de Koter, 1997). Stars 216 and 206 are also too cold. One must then assume that star 214 is hot enough (perhaps an O9.5 V star) to ionize helium.

However, star 214, with its high visual extinction, cannot be at the origin of the spectrum described in Sect. 4, typical of high mass pre-main-sequence objects. Only star 183, or its hidden massive companion if it exists, can be at the origin of this spectrum.

Several other stars are of interest with regard to the ionization of the gas. Star 246 ($A_V = 8$ mag) is the exciting star (B1–B2V) of the separate compact low-brightness H II region located north of Sh 138 (see Fig. 2a). Star 142 ($A_V = 21.7$ mag, with a near-IR excess) is also massive and may participate in the ionization of the H II region.

5.3. The extinction

The Hα and radio maps are different (see Fig. 1), indicating that the extinction is not uniform over the H II region. The optical H II region is triangular in shape; its maximum size in Hα is about 50″ along a southeast–northwest line (1.2 pc for a distance of 5.0 kpc). Star 183 lies at the southeast corner of the optical nebula, 5″ from the radio emission peak. Note that the other massive stars at the cluster's centre (206, 214 and 216) lie even closer to the radio peak. The compact low-brightness H II region surrounding star 246, as well as the Hα filamentary structures in the northwest, are clearly seen on Felli & Harten's (1981) radio map.

The optical brightness fades gradually towards the northwest, as in radio; but it drops abruptly north of a southeast-northwest border line, which is not the case for the radio emission; this very sharp border is clearly due to extinction. The extinction is also high south of Sh 138, where no optical nebular emission is observed, and where a number of highly reddened stars lie. The IR emission between 3 μm and 12 μm has been mapped by ISOCAM (Zavagno 1998). This emission borders the ionized nebula on its south and east sides, and peaks about 12″ south of star 183. Small dust particles situated at the inter-

face between the molecular cloud and the H II region are heated by the radiation field of the cluster and radiate in the mid IR. At optical wavelengths this same dust hides the south and east parts of the H II region.

Comparison of the Hα, radio and dust emission suggests that the Sh 138 H II region is still embedded in a dusty cloud and is partly hidden at visual wavelengths. The young central stars are probably at the origin of a strong wind which has swept the dust and opened a conical aperture in the surrounding cloud through which parts of the H II region are optically visible.

The Hα flux of Sh 138 has been measured in a 134″ diameter diaphragm that encompasses the whole H II region (Caplan et al. 1999). The flux obtained, after correction for the foreground emission, is $F(\mathrm{H}\alpha)$ = 8.86 10^{-12} erg s^{-1} cm^{-2} for the Sh 138 region alone. Assuming $j_\alpha/j_{5\ \mathrm{GHz}}$ = 1.026 10^{-9} erg s^{-1} cm^{-2} Jy^{-1}, and the standard extinction law (Caplan & Deharveng 1986), the observed $F(\mathrm{H}\alpha)$ and S(5 GHz) fluxes correspond to A_V(radio) $\sim$ 5.6 mag. We are far from the visual extinction of 7.6 mag estimated for star 183. Note that this latter extinction, which is deduced from the colour excess of the star assuming the standard extinction law, is independent of the assumed distance, and depends little on the assumed spectral type (between O9 V and B0V). The starlight therefore undergoes two magnitudes of excess visual extinction with respect to that of the Hα emission of the gas. A simple explanation is that there is a significant amount of dust concentrated very close to the star, attenuating the starlight by an additional two magnitudes but having practically no effect on the nebular light.

5.4. The stellar wind associated with star 183

The Paschen decrement observed in the spectrum of star 183 is not compatible with the 'case B' recombination model's predictions which apply to classical H II regions; for example the ratio P12/P19 $= 1.62 \pm 0.24$ (corrected for an A_V of 7.6 mag), differs significantly from the case B value of 3.75 (Hummer & Story 1987). This, plus the fact that all the observed recombination lines are broad, point to the existence of a stellar wind emitted by star 183. The strength of this wind is difficult to estimate. We have used the totally-ionized LTE stellar wind model developed by Nisini et al. (1995) to derive the mass-loss rate from the observed Paschen line fluxes. Assuming a maximum wind velocity of 250 km s^{-1} and an inner radius for the envelope of 8 $R_\odot$, the P12 flux of 1.2 10^{-12} erg s^{-1} cm^{-2} (after correction for $A_V = 7.6$ mag) indicates a mass-loss rate $\dot{M} \approx 3\,10^{-6} M_\odot$ yr^{-1}, typical of high luminosity Herbig Ae/Be stars or embedded YSOs. However this LTE wind model is unable to reproduce the observed Paschen decrement.

Stellar winds are often associated with circumstellar accretion disks. The presence of such a disk around star 183 could explain i) the presence of low excitation emission lines in its spectrum, e.g. the Ca II triplet; ii) the presence of DIBs (Sect. 4.2.1); iii) the excess extinction of star 183 with respect to the surrounding ionized gas (Sect. 5.3); and iv) (possibly) why the spherical, totally-ionized stellar wind model of Nisini et al. (1995) does not reproduce the observed Paschen line ratio. Such a disk seems to exist around the exciting star of the compact H II region Sh 106 (see Bally et al. 1998 for a discussion of this point). However, in the case of star 183, the characteristic evidence for such a disk – a near-IR excess – is not detected.

High-angular-resolution observations of star 183 are obviously needed, to search for both a luminous companion and for a circumstellar disk.

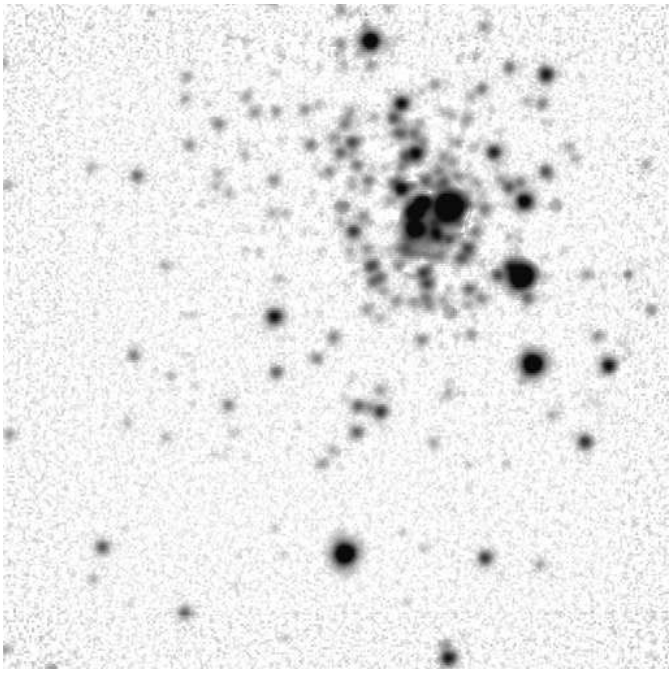


Fig. 9. K image. Same as in Fig. 2, but the extended diffuse emission has been subtracted. We have used logarithmic units to enhance the low brightness stars

5.5. The cluster

The cluster associated with Sh 138 is very conspicuous in Fig. 9, a K image in which the diffuse background has been subtracted. The cluster is centrally concentrated towards the close group of four massive stars discussed previously (183, 206, 214 and 216). This situation is very similar to that observed in a number of young open clusters, where the stellar surface density peaks at the position of the more massive stars (e.g. the Trapezium cluster, Zinneker et al. 1993, McCaughrean & Stauffer 1994; the cluster associated with NGC 2282, Horner et al. 1997; the Monoceros R2 stellar cluster, Carpenter et al. 1997), even when no further evidence for mass segregation is found.

Fig. 10 shows the radial surface density profile. We have used all the stars detected in the K band, without regard to completeness limits. The cluster centre is assumed at the centre of the four massive stars (183, 206, 214, 216) at α_{2000} = 22$^{\mathrm{h}}$ 32$^{\mathrm{m}}$ 45$^{\mathrm{s}}$.6 and δ_{2000} = +58° 28′21″.1. The profile was created by counting stars in 3″ wide circular annuli. The measurements are corrected for the contribution of the field stars, estimated to be 27 stars pc^{-2} at the border of the K frame. However this is probably an overestimate, as we are still very close to

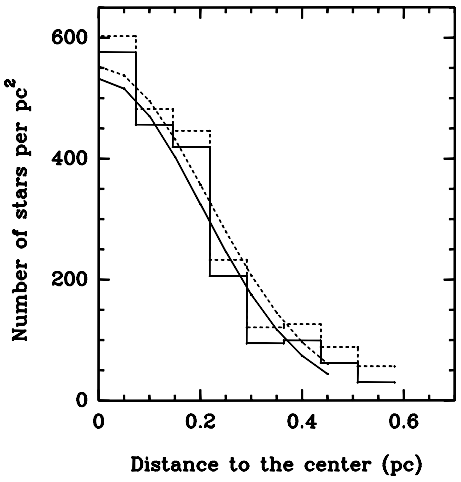


Fig. 10. Stellar surface density distribution as a function of the distance to the centre of the cluster

the cluster. Therefore we show the density profile both *with* (solid line) and *without* (dashed line) this field star correction. Gaussian functions, also shown in Fig. 10, have been adjusted to these distributions by least squares. We obtain a central stellar surface density in the range 530–550 stars pc^{-2}, and a cluster radius in the range 0.24–0.25 pc. The actual central surface density is likely to be higher, as we are missing a number of stars with large extinctions (see Fig. 5a).

This cluster is similar to the Sh 106 cluster (Hodapp & Rayner 1991) in many respects:

• like Sh 106, it is associated with a compact H II region ionized (mainly) by a massive O9-B0 star (IRS 4 for Sh 106),
• the ionizing stars are at the centre of a centrally peaked symmetric cluster, and
• the cluster radius is similar (0.18 pc for Sh 106), as is the stellar surface density. Sh 106 lies much closer (600 pc) than Sh 138 (5000 pc), so that low luminosity stars are more easily detected. Fig. 5 of Hodapp & Rayner (1991) shows that less than one-third of the stars would have been detected if Sh 106 were at the distance of Sh 138 (our K detection limit of $\sim$17 for Sh 138 corresponds to stars with $K \sim 12.4$ in Sh 106); thus the central stellar surface densities are very similar in the two clusters.

Subclustering is observed in the Sh 138 cluster. Star 246 is the exciting star of a compact isolated H II region observed in the northern part; a few very faint K-band stars are observed surrounding this massive star. In the southwest, the massive star 142 also may be at the centre of a small cluster. This star is very reddened ($A_V \sim 28$ mag), is overluminous in K and has a near IR excess. This situation is very similar to that found in the Trapezium cluster: the compact nebula surrounding star 246 corresponds to the compact H II region M 43, situated about 1 pc north of M 42, and star 142 may be the equivalent of the BN-KL IR cluster, corresponding to the youngest population, still embedded in the molecular cloud.

In the Sh 138 cluster, very close stars have very different extinctions; for example, in the central group of massive stars, A_V varies from 7.6 mag (star 183) to more than 27 mag (star 214) in less than 4″. This suggests a very inhomogeneous distribution of dust in the centre of the cluster, which may be due to the presence of disks or accreting envelopes around a number of stars. A highly variable extinction on very small scales was also observed in the cluster associated with the ultra-compact H II region AFGL 4029 (Deharveng et al. 1997).

6. Conclusions

At first sight Sh 138 looks like a classical H II region: it is a thermal radio source and has at its centre an optically bright star which is probably its exciting star. However this photometric and spectroscopic study has shown that the situation is far more complicated.

A very dense cluster at the very centre of the H II region is largely hidden by dust in the visible but appears clearly at longer wavelengths, especially in K. The central surface density of the cluster is around 550 detected stars pc^{-2}, which is very high for a cluster situated ten times farther than the Orion Nebula. At least four O–B2 stars lie at its centre and participate in the ionization of the H II region.

The extinction varies considerably from star to star; very large differences (around 20 mag in A_V) are observed over distances as small as a few arcseconds. Obviously the dust distribution is far from homogeneous: a number of stars situated in the ionized zone are probably still associated with dusty envelopes or disks.

The brightest and probably most massive star, 183, exhibits several characteristics of pre-main-sequence objects such as Herbig Ae/Be stars. Its spectrum displays bright and broad emission lines, evidence for the presence of a strong stellar wind. This star is overluminous at all wavelengths. The presence of a non-resolved massive component could explain this overluminosity.

This study has revealed a number of similarities between this region and two well known objects.

1. Sh 138 with its IR cluster is similar to the compact bipolar H II region Sh 106 (except that Sh 138 is not bipolar). Particularly interesting is the resemblance of the optical spectrum of star 183 to that of IRS 4. IRS 4, of type O9-B0 V and the only exciting star of Sh 106, is clearly associated with an accretion disk.
2. The whole Sh 138 complex is similar to the Orion complex, with its dense cluster, its central Trapezium of massive stars, its surrounding isolated centres of star formation, its molecular environment, etc. We believe that many compact and apparently simple H II regions are in fact as complicated as the nearby Orion Nebula.

Acknowledgements. We would like to thank J. Boulesteix and S. Darbon for providing us with observations of Sh 138 prior to publication, B. Nisini for running calculations of her stellar wind model, L. Johansson for details on CO emission, Y.M. Georgelin for endless discussions about the distances of H II regions, and C. Catala and A.-M. Lagrange for useful suggestions concerning Herbig Ae/Be stars. The referee's helpful suggestions are gratefully acknowledged.

Appendix A: astrometry

The equatorial coordinates of the stars were calculated from the rectangular coordinates furnished by DAOPHOT for the I and K images.

The coordinates of the reference stars were taken from the half-billion-star USNO-A1.0 catalogue (cf. Monet 1997), based (for the northern hemisphere) on the original POSS-I plates, digitized with the Precision Measuring Machine. These data were accessed via the Centre de Données astronomiques de Strasbourg (CDS)[3]. The reference frame is that of the Guide Star Catalog, but the density of objects is more than twenty times greater. Twenty-nine stars over the $4' \times 4'$ I field were used. The position of each of these reference stars was projected onto the plane tangent to an approximate field centre to give 'standard' coordinates X, Y. Then we determined the four parameters (equivalent to change of scale, rotation, x-offset and y-offset) which map X, Y to the observed coordinates x, y in the I image, using the simplest possible model:

$$x = AX - BY + C, \text{and} \quad \text{(A1)}$$

$$y = BX + AY + D. \quad \text{(A2)}$$

The parameters $A, B, C,$ and D were chosen to minimize the sum of the squares of the residual distances in the x, y plane. The formal standard error (quadratically combined error in both coordinates) of the position of one I star is $0\farcs33$. We then used these parameters to calculate the right ascensions and declinations of all the I stars. Sixteen of these I stars which are located in the much smaller field of the K image were then used in the same manner as references to compute the positions of the objects detected in K. The formal standard error of the position of one K star is only $0\farcs08$.

We then merged the two tables of right ascension and declination, giving preference to the K positions when available. The relative positional uncertainty between two stars in the combined table can be considered to be of the order of $0\farcs4$, or only about $0\farcs1$ between two K stars, whereas the absolute uncertainty is essentially that of the GSC, about $1''$.

References

Allamandola L.J., Tielens A.G.G.M., Barker J.R., 1985, ApJ 290, L25
Aspin C., Rayner J.T., McLean I.S., Hayashi S.S., 1990, MNRAS 246, 565
Bally J., Yu K.C., Rayner J., Zinnecker H., 1998, AJ 116, 1863
Beech M., Mitalas R., 1994, ApJSS 95, 517
Bernasconi P.A., Maeder A., 1996, A&A 307, 829
Blitz L., Fich M., Stark A.A., 1982, ApJS 49, 183
Brand J., Blitz L., 1993, A&A 275, 67
Caplan J., Deharveng L., 1986, A&A 155, 297
Caplan J., Deharveng L., Costero R., Peña M., Blondel C., 1999, in preparation
Carpenter J.M., Meyer M.R., Dougados C., Strom S.E., Hillenbrand L.A., 1997, AJ 114, 198
Chan G., Fich M., 1995, AJ 109, 2611
Chevalier C., Ilovaisky S.A., 1991, A&AS 90, 224
Christian C.A., Adams M., Barnes J.V., et al., 1985, PASP 97, 363
Deharveng L., Caplan J., Lombard J., 1992, A&AS 94, 359
Deharveng L., Zavagno A., Cruz-González I., et al., 1997, A&A 317, 459
Deharveng L., Caplan J., Peña M., Costero R., Blondel C., 1999, in preparation
Dubout-Crillon R., 1976, A&AS 25, 25
Felli M., Harten R.H., 1981, A&A 100, 42
Fich M., 1993, ApJS 86, 475
Frogel J.A., Persson S.E., 1972, ApJ 178, 667
Gregory P.C., Taylor A.R., 1986, AJ 92, 371
Hamann F., Persson S.E., 1992a, ApJS 82, 247
Hamann F., Persson S.E., 1992b, ApJS 82, 285
Herbig G.H., Soderblom D.R., 1980, ApJ 242, 628
Hodapp K.W., Rayner J., 1991, AJ 102, 1108
Horner D.J., Lada E., Lada C.J., 1997, AJ 113, 1788
Hummer D.G., Storey P.J., 1987, MNRAS 224, 801
Jenniskens P., Désert F.-X., 1995, In: Tielens A.G.G.M., Snow T.P. (eds.) The Diffuse Interstellar Bands. Astrophys. & Space Science Library 232, 39
Jourdain de Muizon M., d'Hendecourt L., Geballe T.R., 1990, A&A 227, 526
Johansson L.E.B., Olofsson H., Hjalmarson Å., Gredel R., Black J.H., 1994, A&A 291, 89
Kazès A., Le Squeren A.M., Gadéa F., 1975, A&A 42, 9
Kurucz R.L., 1991, In: Crivellari L., Hubeny I., Hummer D.G. (eds.) Stellar Atmospheres: Beyond Classical Models. NATO ASI Series C, Vol. 341, p. 441
Lada C.J., Adams F.C., 1992, ApJ 393, 278
Léger A., Puget J.-L., 1984, A&A 137, L5
Mathis J.S, 1990, ARA&A 28, 37
McCaughrean M.J., Stauffer J.R., 1994, AJ 108, 1382
McGregor P.J., Persson S.E., Cohen J.G., 1984, ApJ 286, 609
Monet D., 1997, BAAS 29, 1235
Nadeau D., Murphy D.C., Doyon R., Rowlands N., 1994, PASP 106, 909
Nisini B., Milillo A., Saraceno P., Vitali F., 1995, A&A 302, 169
Palla F., Stahler S.W., 1990, ApJ 360, L47
Roelfsema P.R., Cox P., Tielens A.G.G.M, et al., A&A 315, L289
Salpeter E.E., 1955, ApJ 121, 161
Schaerer D., de Koter A., 1997, A&A 322, 598
Schmidt-Kaler T., 1982, In: Schaifers K., Voigt H.H. (eds.) Landolt-Bornstein, New series, Group IV, Vol. 2, Springer-Verlag, Berlin, 1
Sellgren K., 1984, ApJ 277, 623
Sharpless S., 1959, ApJS 4, 257
Shaw R.A., Dufour R.J., 1995, PASP 107, 896
Simpson J.P., Rubin R.H., 1990, ApJ 354, 165
Stetson P.B., 1987, PASP 99, 191
Vacca W.D., Garmany C.D., Shull J.M., 1996, ApJ 460, 914
Winkler H., 1997, MNRAS 287, 481
Wouterloot J.G.A., Brand J., Fiegle K., 1993, A&AS 98, 589
Zavagno A., Cox P., Baluteau J.P., 1992, A&A 259, 241
Zavagno A., Deharveng L., Caplan J., 1994, A&A 281, 491 (ZDC)
Zavagno A., 1998, In: Star formation with the Infrared Space Observatory (ISO). ASP Conf. Series 132, 30
Zinneker H., McCaughrean M.J., Wilking B.A., 1993, In: Levy E.H., Lunine J.I. (eds.) Protostars and Planets III. The University of Arizona Press, Tucson & London, p. 429

[3] http://vizier.u-strasbg.fr/cgi-bin/PMM-USNO-A1.0